

Quercia , G.; Spiesz, P.; Hüsken, G.; Brouwers, H.J.H.

Chloride intrusion and freeze-thaw resistance of self-compacting concrete with two different nano-SiO₂

Abstract

In this study two different types of nano-SiO₂ were applied in self-compacting concrete (SCC), both having similar particle size distributions (PSD) but produced in two different processes (pyrogenic and colloidal precipitation). The influence of nano-SiO₂ on transport phenomena in SCC was investigated using the accelerated rapid chloride migration test at different ages (28 and 91 days) as well as the long-term diffusion test. The freeze-thaw resistance, expressed by the scaling factor (Sn), was also studied. Additionally, the microstructural characteristics of the hardened concretes were investigated by FEG-SEM and MIP analyses. The obtained results demonstrate that the addition of 3.8% bwoc of nano-SiO₂ improves the SCC durability due to the refinement of the microstructure and the reduction in the connectivity of the pores. Additionally, a small difference in the reactivity of both types of applied nano-SiO₂ additives was demonstrated.

Keywords: Nano-SiO₂, Concrete, Self Compacting, Durability, Chloride and Freeze-thaw.

Introduction

Durability and sustainability of concrete infrastructure is becoming of critical importance for the construction industry. In this context, SCC is a type of concrete that has generated tremendous interest since its initial development in Japan by Okamura [1]. SCC was developed to obtain durable concrete structures. The aim was to develop a concrete with low yield, moderate viscosity and high resistance to segregation, which also can be cast on-site without compaction. The flow behavior of SCC is obtained by the use of superplasticizers, high amounts of fine particles and, in some cases, a viscosity modifying agent (added to reduce segregation and bleeding). Due to the high amount of fines, the pore structure of SCC differs from the pore structure of traditional concrete. However, the actual application of SCC might be somewhat risky due to the lack of knowledge concerning the actual durability of this material [2].

One of the most referred to and used cementitious nano-materials is amorphous silica with a particle size in the nano-range, even though its application and effect in concrete has not been fully understood yet. It has been reported that nano-SiO₂ addition increases the compressive strength and reduces the overall permeability of hardened concrete due to its pozzolanic properties, which are resulting in finer hydrated phases (C-S-H gel) and densified microstructure (nano-filler and anti-Ca(OH)₂-leaching effects) [3-5]. These effects may enhance the durability of concrete elements and structures. There are different commercial types of nano-SiO₂ additives available on the market, which are produced in different ways such as precipitation, pyrolysis, sol-gel and others [5]. The main characteristics of nano-SiO₂, such as particle size distribution, specific density, specific surface area, pore structure, and reactivity (surface silanol

groups), depend on the production method [3]. Despite the existence of several studies that describe the main properties and characteristics of concrete with nano-SiO₂ particles, most of them focus on the application of nano-SiO₂ as an anti-bleeding and as a compressive strength enhancement additive [3-8]. In the literature, only a few reports on the effects of nano-SiO₂ addition on the durability of SCC are available [9-11]. In addition, the difference in the reactivity of nano-SiO₂ due to its production route has not been reported yet.

In this study two different types of nano-SiO₂ were applied in SCC, both having similar particle size distributions but produced in two different processes (pyrogenic and colloidal precipitation). The influence of nano-SiO₂ on chloride transport of SCC was investigated using the accelerated rapid chloride migration test at different ages (28 and 91 days) as well as the long-term diffusion test. The freeze-thaw resistance, expressed by the scaling factor (Sn), was also studied. Additionally, the microstructural characteristics of the hardened concretes were investigated by FEG-SEM and MIP analyses.

Materials and methods

Materials and SCC mix design

The Portland cement used in this study was CEM I 42.5N (ENCI, The Netherlands), as classified by [12]. This cement consists of at least 95% of Portland cement clinker; the initial setting time is 60 min, the water demand amounts to 38.9% by weight, and the compressive strength after 2 days is 21 ± 3 N/mm² and 51 ± 4 N/mm² at 28 days [12]. The coarse aggregates used were composed of broken granite in fractions 8-16 mm and 2-8 mm. Two different sands were used: dredged river sand (0-4 mm) and microsand, composed mainly of natural sandstone waste (0-1 mm) collected during the crushing process of coarser fractions. Ground limestone powder was applied as a filler. Two different commercial nano-SiO₂ additives were selected to produce two different SCC batches: one colloidal nano-SiO₂ suspension and one fumed powder nano-SiO₂. Both nano-SiO₂ have similar PSDs and specific surface areas measured by BET (Brunauer-Emmet-Teller method [13]), following the standard DIN-ISO 9277-2005 [14]. Furthermore, one superplasticizer (SP) of the 3rd generation, based on polycarboxylate ethers was added in order to adjust the workability of the mixes. A summary of the general characteristics of all materials used in this study is shown in Table 1 and their PSDs are depicted in Fig. 1.

For the composition of SCC mixes, the mix design concept described in [15] was used. This design concept makes use of an optimization algorithm described in [16] in order to compose the mix proportions of all solid ingredients of the concrete mix, following the theory of continuously graded granular mixtures. In the optimization process, the distribution modulus (q) of 0.25 was used together with the following constraints: cement content of 340 kg/m³, w/c ratio 0.45 and air content in the fresh mix of 1% by volume. The cement content and the w/c ratio were selected based on NEN-EN 206-1 (2008) [17] for XS3 exposure class (exposition to chlorides originating from seawater). In addition, the flow class F7 (630-800 mm) of fresh SCC was selected as target, taking into account the Dutch recommendation BRL 1801 [18] for SCC. An example of the target curve and the composed SCC mix grading curve is shown in Fig.

1. The final mix proportioning and characteristics of the reference mix without nano-SiO₂ and two mixes with nano-SiO₂ addition are presented in Table 2.

Table 1
Properties of used materials

Materials	Specific density [g/cm ³]	BET [m ² /g]	pH	Solid content [% w/w]	Loss on ignition [L.O.I]	Computed SSA [m ² /m ³]
CEM I 42.5N	3.14	1	-	-	2.8	1,699,093
Colloidal nano-SiO ₂	1.40	50	9.5	50	-	46,110,081
Powder nano-SiO ₂	2.15	56	5.0*	-	0.5	48,175,461
Limestone powder	2.71	-	-	-	-	1,234,362
Microsand (sandstone)	2.64	-	-	-	-	193,514
Sand 0-4	2.64	-	-	-	-	14,251
Granite 2-8	2.65	-	-	-	-	1,740
Granite 8-16	2.65	-	-	-	-	515
Superplasticizer	1.10	-	7.0	35	-	-

(*) 4% w/w in water

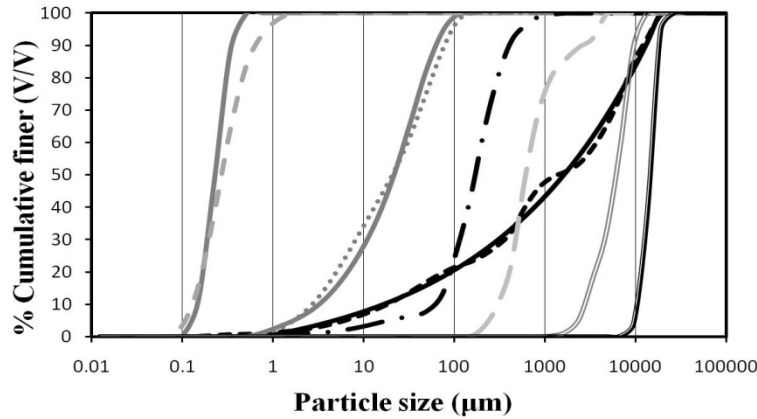


Fig. 1
PSD of materials used and target function based on [18]

Table 2
Composition and characteristics of the designed SCC mixes

Materials	Reference	Colloidal nano-SiO ₂	Powder nano-SiO ₂
	[kg/m ³]		
CEM I 42.5N	340.0	340.0	340.1
Nano-SiO ₂	0.0	12.8	12.8
Limestone powder	179.4	151.8	151.9
Microsand (sandstone)	125.0	141.3	141.4
Sand 0-4	624.3	617.9	618.0
Granite 2-8	733.8	735.6	735.7
Granite 8-16	274.7	274.2	274.3
Water	153.0	153.0	153.0
SP	3.4	6.5	6.5
Air [% V]-estimated	1.0	1.0	1.0
Density [g/cm ³]	2.427	2.427	2.430
w/c	0.45	0.45	0.45

w/p	0.267	0.270	0.270
Powder content [dm ³ /m ³]	194.2	192.7	192.6
Composed surface [m ² /m ³]	277,972	547,905	554,428
SP content [g/m ²]	0.0122	0.0119	0.0117
SP content [% bwoc]	1.0	1.9	1.9
Slump flow [mm]	690 - 720	664 - 701	685 - 720
V-funnel time [s]	35.0	20.5	24.5
Fresh density [g/cm ³]	2.399	2.384	2.392
Air content [%V]*	1.15	1.79	1.58
Packing density [%]*	83.55	82.91	83.12
Total Permeable porosity [%] ^ξ	12.07	12.45	12.48
Depth of penetration of water under pressure [mm] ⁺	26	3	3
28-days splitting tensile strength [MPa] ^ψ	4.51	4.92	5.48
28-days compressive strength [MPa] ^ψ	78.2	87.7	78.5
91-days compressive strength [MPa] ^ψ	83.5	92.2	91.0

bwoc: Based on the weight of cement, * Calculated value, (ξ) Vacuum saturation technique, (+)Tested according to BS-EN 12390-8 [19] after 28 days, (ψ)Tested according to BS-EN 12390-2 [20], BS-EN 12390-3 [21], BS-EN 12390-6 [22]

Test methods

For the rapid chloride migration test (RCM), three cores (diameter of 100 mm, height of 150 mm) were drilled from three cubes for each mix. Two specimens for the RCM test were retrieved from each core, giving in total six test specimens (cylinders having a diameter of 100 mm and a height of 50 mm) for each mix. Three of these specimens were tested at the age of 28 days and the remaining three at the age of 91 days. One day prior to the RCM test, the specimens were pre-conditioned (vacuum-saturation with limewater). The RCM test was performed according to NT Build 492 [23] and the test set-up used is described in detail in [24]. The duration of the RCM test for all samples was 24 hours. After the test, the penetration depth of chlorides was measured on split samples by applying a colorimetric indicator for chlorides (0.1 M AgNO₃ solution) and subsequently, the values of the chloride migration coefficients (D_{RCM}) were calculated according to [23].

Prior to the RCM test, the electrical resistance was measured on the same samples by using the so-called ‘two electrodes’ method [25]. For this, an AC test signal ($f = 1$ kHz) was applied between two stainless-steel electrodes and the resistance of the concrete sample placed between the electrodes was measured. Finally, the conductivity of the samples was calculated taking into account their thickness and transversal area.

As the addition of nano-SiO₂ changes the ionic strength, the pH and the conductivity of the pore solution [26], the results obtained using the RCM test may be influenced, as the procedure of this test is based only on experience with OPC systems [27]. On the contrary, the natural diffusion test is only affected by the pore structure (permeability and tortuosity), chloride binding and the chloride concentration gradient. Thus, the chloride diffusion test may be more reliable for SCC with nano-SiO₂ addition than the RCM test. Based on this, a chloride diffusion test was performed. For each prepared mix, three specimens (cylinders having a diameter of 100 mm and a height of 50 mm) were extracted from different cubes. The diffusion test began 28 days after casting the cubes, following the procedure described in [28]. Prior to the test, all

external faces of the specimens were coated with an epoxy resin except for one flat surface, left uncovered to allow the chlorides to penetrate the samples just from that side. Then, the specimens were immersed in a sodium chloride solution (concentration of 165 g/dm^3) for 63 days, at room temperature, in a sealed and de-aired container, with the uncoated surface on top. After the exposure period, one specimen from each test series was split in order to measure the penetration depth of chlorides (using 0.1 M AgNO_3 solution as a colorimetric chloride indicator). The remaining samples were dry-ground in layers for determining the chloride concentration profiles. The grinding was performed on an area of 73 mm in diameter using the Profile Grinder 1100 (Germann Instruments). The obtained powder was collected for the determination of the total chloride concentration profiles, following the procedure described in [29]. An automatic potentiometric titration unit was used for the Cl^- concentration measurements, applying a 0.01 M AgNO_3 as titrant. The obtained chloride concentration profiles were fit to the solution of Fick's 2nd law, in order to estimate the apparent chloride diffusion coefficient (D_{app}) and the concentration of chloride near the surface.

As a further durability assessment, the freeze-thaw test was performed on SCC samples, even though their air content in the fresh mix was less than the recommended value of 4% by volume [17]. The freeze-thaw resistance, expressed by the surface scaling factor (S_n), was determined following NEN-EN 12390-9 [30]. Nevertheless, the test samples differed from the specifications in the standard – for practical reasons cylinders were used instead of slabs. The 150 mm cubes were cured under water after demolding until the age of 14 days, when the cores (100 mm in diameter) were extracted and sliced (two cylinders of 50 mm in height were obtained from each core). Afterwards, the obtained cylinders were cured and sealed after 25 days with tight rubber sleeves. The sealed samples were placed in a polyurethane insulation of 10 mm thickness and surface-saturated with demineralized water for three days. Three specimens were tested for each mix, resulting in a total exposed surface area of 0.024 m^2 . After saturating the samples, the demineralized water was replaced by a 3 mm layer of 3% by mass NaCl solution, poured on the top surface of the samples and the freeze-thaw cycles were started. The applied temperature profile was following the recommendations given in NEN-EN 12390-9 [30]. The level of the solution on the surface of the concrete was adjusted regularly. In total, 56 freeze-thaw cycles were performed, during which the surface scaling was measured after 7, 14, 28, 42 and 56 cycles.

The pore size distribution was measured using the mercury intrusion porosimetry (MIP) technique (Autopore IV, Micromeritics). The maximum applied pressure of the mercury was 228 MPa and the equilibrium time was 20 seconds. The pore size in the range of $900 - 0.005 \mu\text{m}$ was investigated. Pieces of hardened paste (approximately 2 grams), extracted from SCC samples were tested.

Finally, the microstructural morphology of the prepared concrete was analyzed using a high resolution scanning electron microscope (FEI Quanta 600 FEG-SEM) with a Schottky field emitter gun (at voltage of 10 keV and 0.6 mbar of low-vacuum pressure). Furthermore, a general chemical analysis was performed using EDAX energy dispersive spectroscopy (EDS).

Results and discussion

Fig. 2a shows the average values of the conductivity, measured on cylindrical SCC samples that were extracted from the cast cubes. It is clearly shown that the conductivity of the SCC with nano-SiO₂ addition is reduced by more than 50% compared to the SCC reference mix. Meanwhile, the SCC with the colloidal nano-SiO₂ presented a slightly lower conductivity than samples with the powder nano-SiO₂. This behavior is an indication of the ability of the water-saturated pore structure of the concrete to transport electrical charge. Different authors [31,32] established that the conductivity is directly related to the porosity, pore structure (tortuosity, connectivity and conductivity) and to the pH of the pore solution (pH value is lower in presence of nano-SiO₂). In general, higher porosity reflects on a higher conductivity due to the presence of a larger volumetric fraction of liquid-saturated pores. The lower conductivity values measured on the SCC with nano-SiO₂ are caused by the pore structure refinement (less connected pores) due to the progressive pozzolanic reaction and a higher hydration degree (see the microstructural analysis section). The small difference between the two types of silica is mainly related to the higher reactivity of the colloidal nano-SiO₂, which promotes a more compact and finer microstructure (higher stiffness C-S-H gel) than the powder nano-SiO₂. Conductivity can also be related to the compressive strength as it was demonstrated by Andrade et al. [33].

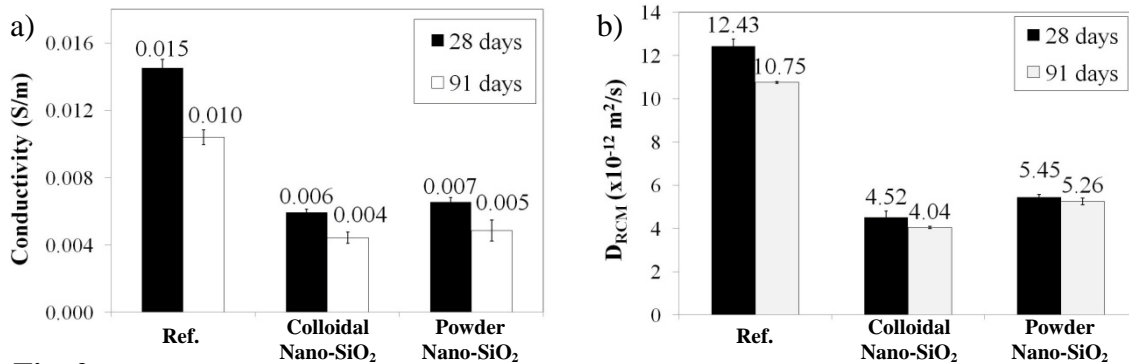


Fig. 2
28 and 91 days results of the tested SCC mixes, a) conductivity, b) chloride migration coefficient (D_{RCM})

Fig. 2b presents the average values of the calculated chloride migration coefficients (D_{RCM}) of each tested SCC. As the conductivity test results, the migration coefficients are much lower for the mixes containing nano-SiO₂. In this context, the SCC mix with the colloidal nano-SiO₂ shows the best performance. The explanation of this behavior is the same as previously discussed for the conductivity test results. A finer porosity, greater tortuosity and more precipitated C-S-H gel reduces the ingress speed of chloride into the concrete. The 28 days D_{RCM} can be employed in service life design codes [34, 35] for concrete elements and structures exposed to chlorides. When comparing all the obtained 28 days D_{RCM} with the values suggested in CUR Durability Guideline [35] for 100 years of service life (Table 3), the SCC reference mix is out of the range of the aimed exposure class XS3. On the contrary, both SCC mixes with nano-SiO₂ addition satisfied the exposure class XS3 with a concrete cover depth of 50 mm. On the other hand, comparing the obtained D_{RCM} values to similar SCC mixes published in literature, the values obtained for the reference mix are in line with SCC mixes containing high

amount of limestone powder (between 8 and $12 \times 10^{-12} \text{ m}^2/\text{s}$ at 28 days [2]), meanwhile the values obtained for the SCC mixes with nano-SiO₂ addition are comparable to reported values of SCC composed of slag cement or fly ash with similar w/b ratio and cement content (between 4 and $5 \times 10^{-12} \text{ m}^2/\text{s}$ [2]).

Table 3
Maximum values of 28-days D_{RCM} coefficients for 100 years of service-life design of concrete, taken from [35].

Minimum concrete cover depth [mm]		Maximum value of $D_{RCM} [\times 10^{-12} \text{ m}^2/\text{s}]$							
steel	pre-stressed steel	CEM I		CEM I + CEM III 25 - 50 % GGBS		CEM III 50 – 80 % GGBS		CEM II B/V + CEM I 20-30 % fly ash	
		XD1, XD2, XD3, XS1	XS2, XS3	XD1, XD2, XD3, XS1	XS2, XS3	XD1, XD2, XD3, XS1	XS2, XS3	XD1, XD2, XD3, XS1	XS2, XS3
35	45	3.0	1.5	2.0	1.0	2.0	1.0	6.5	5.5
40	50	5.5	2.0	4.0	1.5	4.0	1.5	12	10
45	55	8.5	3.5	6.0	2.5	6.0	2.5	18	15
50	60	12	5.0	9.0	3.5	8.5	3.6	26	22
55	65	17	7.0	12	5.0	12	5.0	36	30
60	70	22	9.0	16	6.5	15	6.5	47	39

In Fig. 3a the obtained apparent chloride diffusion coefficients (D_{app}) of the three SCC mixes are shown. A trend similar to the D_{RCM} was obtained for the diffusion test. The largest D_{app} was computed for the reference SCC ($9.61 \times 10^{-12} \text{ m}^2/\text{s}$). The D_{app} of $4.45 \times 10^{-12} \text{ m}^2/\text{s}$ and $3.55 \times 10^{-12} \text{ m}^2/\text{s}$ were obtained for powder nano-SiO₂ and colloidal nano-SiO₂, respectively.

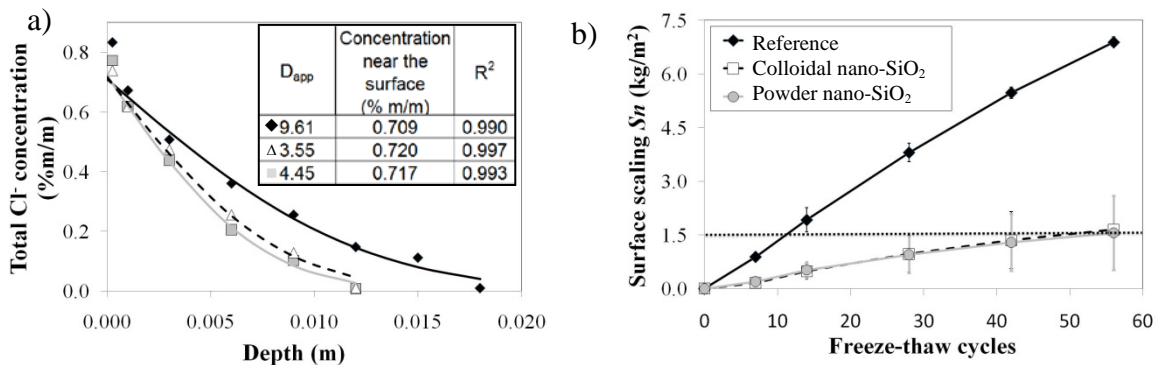


Fig. 3
a) Chloride diffusion profiles of the tested SCC mixes, b) Cumulative scaling factor (S_n) after 56 freeze-thaw cycles (3% NaCl solution).

The results of the freeze-thaw surface scaling test of the three selected SCC mixes are shown in Fig. 3b. The failure of the SCC reference mix, taking into account a maximum scaling of 1.5 kg/m^2 at 28 cycles as recommended in [36], occurred about the 11th cycle.

In contrary, the SCC mixes with nano-SiO₂ addition resulted in a surface scaling factor lower than the recommended value for non-air entrained concrete after 28 cycles. These SCC mixes failed the 1.5 kg/m² criteria after 48 cycles. On the contrary to the other properties determined, the SCC with powder nano-SiO₂ addition showed slightly better behavior than the SCC with colloidal nano-SiO₂. The freeze-thaw resistance depends on the compressive strength, porosity, air content and other parameters such as the air-bubbles distribution and pore size [37]. A better resistance to the freeze-thaw cycles of the SCC with nano-SiO₂ addition can be attributed to its denser and more compacted microstructure. The highly stiff C-S-H gel and the refined pore structure results in a limited intrusion of water and in an improved resistance to changes of temperature near the surface of the concrete. Despite the better freeze-thaw resistance of the SCC with nano-SiO₂ compared to the reference mix, its scaling values are larger than the recommended value of 0.5 kg/m² after 56 cycles, suggested by Stark and Wicht [38] for concrete classified as having good resistance against freeze-thaw exposure. Nevertheless, with an air entrainment admixture that guaranties a minimum air content of 4%, the freeze-thaw resistance of SCC with nano-SiO₂ should result in a mix having a high resistance to freeze-thaw.

To support the previous findings, the hardened paste samples were analyzed using mercury intrusion porosimetry (MIP). The obtained results are shown in Table 4 and Fig. 4. It is evident from the data an addition of 3.8% of nano-SiO₂ slightly increased the volume of pores lower than 20 nm. Similar trends were obtained analyzing the overall parameters extracted from the mercury intrusion test. These parameters are shown in Table 3. It is clearly displayed in Table 3 that the addition of nano-SiO₂ decreased the median pore diameter (by volume and area) and the average pore diameter, which is reduced from 27.8 nm (for the reference) to 24.3 and 25.9 nm for the colloidal and powder nano-SiO₂, respectively. Apparently, a reduction of 3.5 nm in the average pore diameter was enough to increase the properties of the SCC with nano-SiO₂ addition. Another interesting fact, also presented in Table 3, is that the apparent density of the hardened paste was higher for the SCC with nano-SiO₂ (both types). This demonstrates that the addition of nano-SiO₂ promotes the densification of the cement matrix. Despite the densification of the cement matrix, the porosity increases with the addition of nano-SiO₂ (see Table 4). This means that other factors are improving the durability of the SCC with nano-SiO₂. These factors can be e.g. changes of the shape of the pores (cylindrical vs. bottle-neck type), changes of the tortuosity or the connectivity and an improvement of the ITZ of cement paste/aggregates. Further research is needed to address this topic in the future.

Table 4
Properties of the hardened paste of SCC mixes obtained from MIP measurements

Properties	Reference	Colloidal nano-SiO ₂	Powder nano-SiO ₂
Median pore diameter volume [nm]	34.8	30.9	33.8
Median pore diameter area [nm]	20.3	17.2	17.5
Average pore diameter (4V/A) [nm]	27.8	24.3	25.9
Apparent density [g/ml]	2.41	2.44	2.45
Porosity [%]	8.79	9.31	8.99

All SCC mixes were analyzed in a low vacuum environment (0.6 mbar) using FEG-SEM device. The objective of this analysis was to support the findings shown in the present research. In this context, Fig. 5 shows some morphological characteristics of the microstructure of the SCC reference mix. The SCC reference mix has a dense microstructure and a relatively good ITZ (Fig. 5a). Nevertheless, its microstructure is heterogeneous, with high amount of small pores and big sized C-S-H gel structures. Additionally, acicular (rod like) structures (Fig. 5b) were identified and possibly formed of Ettringite needles and other AFt phases that are rich in CO_3^{2-} . The formation of the rod-like AFt phases in cement paste with high calcium carbonate concentration was reported in [39]. In addition, well crystallized hexagonal Portlandite (Ca(OH)_2) plates were clearly precipitated in the cement matrix and in the largest air pores (Fig. 5c). Normally, the presence of high amounts of Ca(OH)_2 results in a lower chloride intrusion resistance and lower compressive strength. These findings are in line with the mechanical and durability test results discussed previously.

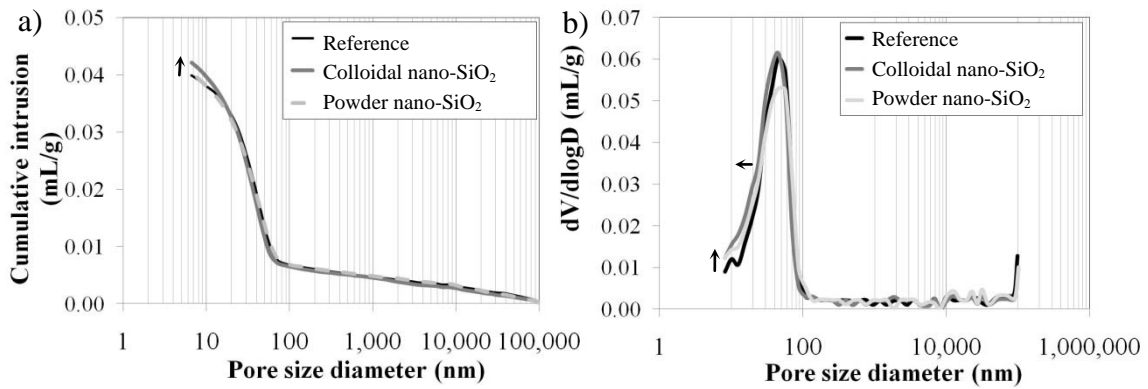


Fig. 4
Mercury intrusion porosimetry results of hardened paste extracted from the tested SCC mixes, a) Cumulative intrusion vs. pore size curves, b) Log differential intrusion vs. pore size curves.

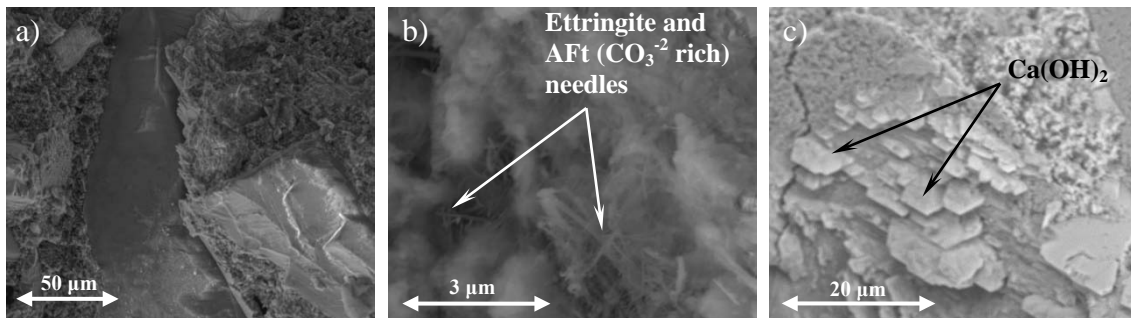


Fig. 5
FEG-SEM photomicrographs of SCC reference mix, a) cement matrix and aggregate ITZ, b) rod like calcium carboaluminate hydrate or Ettringite needle and c) precipitated hexagonal Portlandite plate crystals.

As it can be observed in Fig. 6a, the SCC with colloidal nano-SiO₂ addition shows a more homogeneous microstructure compared to the reference mix. This microstructure is characterized by compact and small sizes of C-S-H gel morphology. As a

consequence, a denser ITZ was also confirmed by SEM (Fig. 6b). It is important to notice that the rod or needle-type precipitates, or well precipitated $\text{Ca}(\text{OH})_2$ crystals were not found in the microstructural analysis. This confirms that the addition of the nano- SiO_2 causes a refinement of the microstructure and induces precipitation of small and high stiffness sized C-S-H gel. In addition, the resistance to chloride intrusion was enhanced because of the densification of the microstructure and the high specific surface area of the gel [26]. The high reactivity of the colloidal nano- SiO_2 was also confirmed by Fig. 6c, where small C-S-H gel precipitates were observed around the limestone powder and agglomerates of nano-particles.

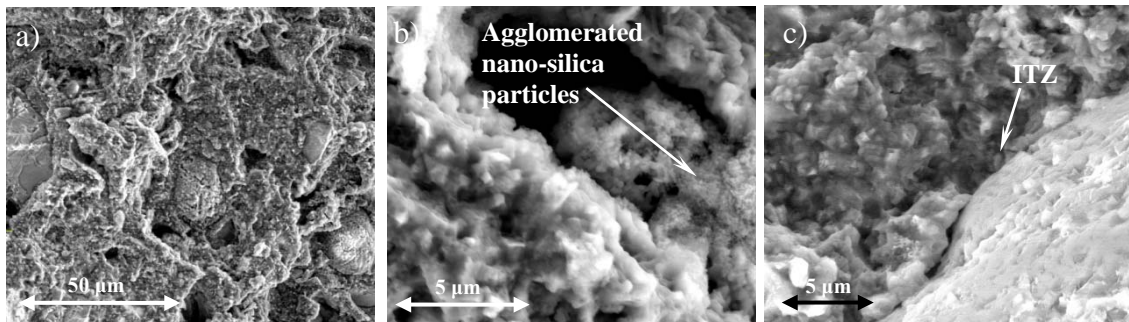


Fig. 6
FEG-SEM photomicrographs of SCC colloidal nano- SiO_2 mix, a) cement matrix, b) agglomerates in a pore and c) aggregate dense ITZ.

Also in the case of SCC with powder nano- SiO_2 , a similar microstructural analysis was performed. Its microstructure is also found to be refined (Fig. 7a), but not as much as with the colloidal nano- SiO_2 . Apparently, due to the fact that this nano- SiO_2 was produced at high temperature (more compact, lower concentration of silanol groups) its pozzolanic reactivity is lower than the colloidal one. Nevertheless, a relatively homogeneous matrix was observed with more small distributed pores (Fig. 7b). Even though the microstructure was refined due to the addition of the powder silica, it was still possible to observe some remnant rod-like AFt phases in the matrix (Fig. 7c).

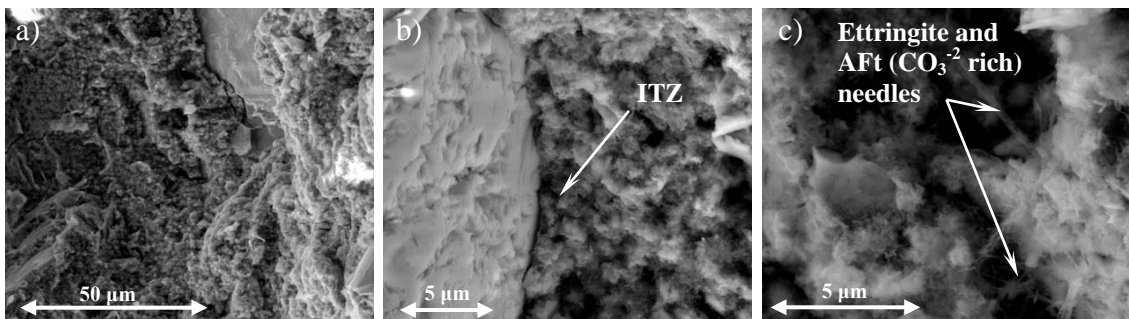


Fig. 7
FEG-SEM photomicrographs of SCC powder nano- SiO_2 mix, a) cement matrix, b) aggregates ITZ and c) rod like precipitates.

The differences observed in the microstructural analysis can explain the results that were obtained for the two SCC with both types of nano- SiO_2 addition, where the SCC

containing colloidal nano-SiO₂ presented better results in most of the performed tests. The SCC with colloidal nano-SiO₂ showed a denser matrix and a better ITZ than the SCC with powder nano-SiO₂. In addition, a refined microstructure was obtained (no Ettringite needles were found). This refinement causes better mechanical and durability properties of the tested SCC.

4. Conclusions

Based on the test results obtained from a reference SCC and mixes containing two types of nano-SiO₂, the following conclusions can be drawn:

All durability indicators of the SCC studied (conductivity, chloride migration and diffusion coefficients, and freeze-thaw resistance) were significantly improved with the addition of 3.8% of both types of the nano-SiO₂. Moreover, the SCC with colloidal nano-SiO₂ showed slightly better properties than the SCC with powder nano-SiO₂.

The microstructural analysis of the hardened SCC reveals that the addition of nano-SiO₂ resulted in a homogeneous microstructure, characterized by compact and small sized C-S-H gel. As a consequence, a denser ITZ was produced. The addition of nano-SiO₂ caused a refinement of the microstructure (less interconnected pore structure) and induced precipitation of small sized C-S-H gel having high stiffness. This was also confirmed by MIP measurements. In addition, the resistance against chloride intrusion was enhanced because of the densification of the microstructure. The high reactivity and faster pozzolanic behavior of the colloidal nano-SiO₂ particles at early age produced a more refined microstructure than obtained for the SCC with powder nano-SiO₂.

Acknowledgements

This research was carried out under the project number M81.1.09338 in the framework of the Research Program of the Materials innovation institute M2i and The European Community's Seventh Framework Program, ProMine: Nano-particle products from new mineral resources in Europe, FP7-NMP-2008-LARGE-2 under grant agreement 228559. The authors also wish to express their gratitude to the following sponsors of the Building Materials research group at TU Eindhoven: Rijkswaterstaat Centre for Infrastructure, Graniet-Import Benelux, Kijlstra Betonmortel, Struyk Verwo, Attero, Enci, Provincie Overijssel, Rijkswaterstaat Directie Zeeland, A&G Maasvlakte, BTE, Alvon Bouwsystemen, V.d. Bosch Beton, Selor, Twee "R" Recycling, GMB, Schenk Concrete Consultancy, Intron, Geochem Research, Icopal, BN International, APP All Remove, Consensor, Eltomation, Knauf Gips, Hess ACC Systems and Kronos (chronological order of joining).

References

- [1] Okamura, H. and Ozawa, K. "Mix-design for self-compacting concrete", Concrete Library, Japanese Society of Civil Engineers- JSCE Vol. 25 (1995), pp. 107-120.
- [2] Audenaert, K., Boel, V. and De Schutter, G. "Chloride migration in self compacting concrete", Proceeding Fifth International Conference on Concrete under Severe Conditions: Environment and Loading (CONSEC'07). June 4-6 (2007), Tours, France, pp. 191-298.
- [3] Sobolev, K., Flores, I. and Hermosillo, R. "Nanomaterials and Nanotechnology for High-performance cement composites, Proceedings of ACI Session on Nanotechnology of Concrete: Recent Developments and Future Perspectives", November 7 (2006), Denver, U.S.A., pp. 91-118.
- [4] Nili, M., Ehsani, A. and Shabani, K. "Influence of nano-SiO₂ and micro-silica on concrete performance", Proceedings Second International Conference on Sustainable Construction Materials and Technologies. June 28-30 (2010). Universita Ploitecnica delle Marche, Ancona, Italy, 2010, pp. 1-5.
- [5] Quercia, G. and Brouwers, H.J.H. "Application of nano-silica (nS) in concrete mixtures", In Gregor Fisher, Mette Geiker, Ole Hededal, Lisbeth Ottosen, Henrik Stang (Eds.), 8th fib International Ph.D. Symposium in Civil Engineering. Lyngby, June 20-23 (2010), Denmark, pp. 431-436.
- [6] Green, B.H. "Development of a high-density cementitious rock-maching grout using nano-particles", "Proceedings of ACI Session on "Nanotechnology of Concrete: Recent Developments and Future Perspectives", November 7, Denver, USA (2006), pp. 119-130.
- [7] Collepardi, M., Ogoumah, J.J., Skarp, U. and Troli, R. "Influence of amorphous colloidal silica on the properties of self-compacting concretes", Proceedings of the International Conference "Challenges in Concrete Construction - Innovations and Developments in Concrete Materials and Construction", Dundee, Scotland, UK, 9-11 September (2002), pp. 473-483.
- [8] Sadrumontazi, A. and Barzegar, A. "Assessment of the effect of Nano-SiO₂ on physical and mechanical properties of self-compacting concrete containing rice husk ash", Proceedings Second International Conference on Sustainable Construction Materials and Technologies. June 28-30 (2010). Universita Politecnica delle Marche, Ancona, Italy, 2010, pp. 1-9.
- [9] Maghsoudi, A.A. and Arabpour-Dahooei, F. "Effect of nanoscale materials in engineering properties of performance self compacting concrete", Proceeding of the 7th International Congress on Civil Engineering. Iran (2007). pp. 1-11.
- [10] Raiess-Ghasemi, A.M., Parhizkar, T. and Ramezaniapour, A.A. "Influence of colloidal nano-SiO₂ addition as silica fume replacement material in properties of concrete", Proceedings Second International Conference on Sustainable Construction Materials and Technologies. June 28-30 (2010). Universita Ploitecnica delle Marche, Ancona, Italy, 2010, pp. 1-8.
- [11] Wei, X. and Zhang P. "Sensitivity analysis for durability of high performance concrete containing nanoparticles based on Grey Relational Grade". Modern Applied Science Vol. 5, No.4, August (2011), pp. 68-73.
- [12] ENCI B.V. "Betonpocket 2010", Heidelberg Cement Group, 's-Hertogenbosch (2009), The Netherlands (in Dutch), pp. 1-288.

- [13] Brunauer, S., Emmet, P.H. and Teller, E. "Adsorption of gases in multimolecular layers", *Journal of American Chemical Society* 62 (1938). pp. 309-319.
- [14] DIN ISO 9277. "Determination of the specific surface area of solids by gas adsorption using the BET method", German Institute of Normalization-DIN (2005). pp. 1-19.
- [15] Hunger, M. "An Integral Design Concept for Ecological Self-Compacting Concrete", Ph.D. Thesis, Eindhoven University of Technology (2010). The Netherlands.
- [16] Hüsken, G. and Brouwers, H.J.H. "A new mix design concept for earth-moist concrete: A theoretical and experimental study", *Cement and Concrete Research* 38 (2008). pp. 1246-1259.
- [17] Dutch Normalization-Institute. *Nederlandse invulling van NEN-EN 206-1: Beton Deel 1: Specificatie, eigenschappen, vervaardiging en conformiteit*, Nederlands Normalisatie Instituut, Delft (2008), The Netherlands. pp. 1-72.
- [18] BMC Certificatie BRL 1801: Nationale Beoordelingsrichtlijn Betonmortel. BMC Certificatie, Gouda (2006), The Netherlands (in Dutch).
- [19] BS-EN 12390-8. "Testing hardened concrete - Depth of penetration of water under pressure", British Standards Institution-BSI and CEN European Committee for Standardization (2009), pp 1-10.
- [20] BS-EN 12390-2. "Testing hardened concrete - Part 2: Making and curing specimens for strength tests", British Standards Institution-BSI and CEN European Committee for Standardization (2000), pp. 1-10.
- [21] BS-EN 12390-3. "Testing hardened concrete - Compressive strength of test specimens", British Standards Institution-BSI and CEN European Committee for Standardization (2009), pp. 1-22.
- [22] BS-EN 12390-6. "Testing hardened concrete - Tensile splitting strength of test specimens", British Standards Institution-BSI and CEN European Committee for Standardization (2000), pp 1-14.
- [23] Nordtest method NT Build 492. "Concrete, mortar and cement-based repair materials: Chloride migration coefficient from non-steady-state migration experiments". Finland (1999), pp. 1-8.
- [24] Spiesz P., Ballari M.M., Brouwers H.J.H. "RCM: A new model accounting for the non-linear chloride binding isotherm and the non-equilibrium conditions between the free- and bound-chloride concentrations", *Construction and Building Materials* 27 (2012), pp. 293-304.
- [25] Polder, R.B. "Test methods for on site measurement of resistivity of concrete a RILEM TC-154 technical recommendation", *Construction and Building Materials* 15 (2001), pp. 125-1301.
- [26] Bentz, D.P., Jensen, O.M., Coats, A.M. and Glasser, F.P. "Influence of silica fume on diffusivity in cement-based materials I. Experimental and computer modelling studies on cement pastes", *Cement and Concrete Research* 30 (2000), pp. 953-962.
- [27] Tang, L. Chloride transport in concrete – measurement and prediction. PhD Thesis, 1996, Chalmers University of Technology, Gothenburg, Sweden.
- [28] Nordtest method NT Build 443. "Concrete, hardened: Accelerated chloride penetration". Finland (1995), pp. 1-5.
- [29] Yuan, Q. "Fundamental studies on test methods for transport of chloride ions in cementitious materials", PhD thesis, Universiteit Gent, Belgium (2009), pp. 1-340.

- [30] NEN-EN 12390-9. “Testing hardened concrete - Freeze-thaw resistance – Scaling”, CEN European Committee for Standardization and Dutch Normalization-Institute, Delft (2006), The Netherlands (in English), pp. 1-29.
- [31] Desmet, D., Hernandez, J., Willain, L. and Vantomme, J. “Porosity determination of self-compacting concrete using forced saturation”, Proceeding of the XIII International Conference on Cement Chemistry, Madrid, July 4-8 (2011). pp 1-7.
- [32] Andrade, C., D’Andrea, R., Lopez, J.C., Cienfuegos-Jovellano, A., Alvarez, J.M. and Millan J.M. “Use of electrical resistivity as complementary tool for controlling the concrete production”, Proceeding of the XIII International Conference on Cement Chemistry, Madrid, July 4-8 (2011). pp 1-7.
- [33] Andrade, C., Rio, O., Castillo, A., Castellonte, M. and D’ Andrea, R. “A NDT Performance method based on electrical resistivity for the specification of concrete durability”, ECCOMAS Thematic Conference on Computational Methods in Tunnelling, Vienna, Austria, August 27-29 (2007), pp. 1-9.
- [34] DuraCrete. “Probabilistic Performance based Durability Design of Concrete Structures”, DuraCrete Final Technical Report (2000). Document BE95–1347/R17.
- [35] CUR Durability Guideline. Duurzaamheid van constructief beton met betrekking tot chloride-geïnitieerde wapeningscorrosie. CUR Bouw en Infra. (2009), Gouda, The Netherlands (in Dutch). pp. 1-65.
- [36] Romero, H.L., Casati, M.J., Galvez, J.C., Molero, M. and Segura, I. “Study of the damage evolution of concrete under freeze-thaw cycles using traditional and non-traditional techniques”, Proceeding of the XIII International Conference on Cement Chemistry, Madrid, July 4-8 (2011). pp 1-7.
- [37] Neville, A. M. “Properties of Concrete”, 4th ed. (2002), Prentice Hall/Pearson, Harlow, U.K. pp. 537-576.
- [38] Stark, J. and Wicht, B. Dauerhaftigkeit von Beton: Der Baustoff als Werkstoff, Birkhäuser, Basel. (2001), Switzerland (in German).
- [39] Nocun-Wczelik, W. and Loj, G. “Effect of finely dispersed limestone additives of different origin on cement hydration kinetics and cement hardening”, Proceeding of the XIII International Conference on Cement Chemistry, Madrid, July 4-8 (2011). pp 1-7.

Authors

Dipl.-Ing. George Quercia, MSc.
 Material innovation institute (M2i)
 Eindhoven University of Technology
 Faculty of the Built Environment
 P.O. Box 513
 5600 MB Eindhoven
 E-mail: g.quercia-bianchi@m2i.nl

Prof.dr.ir. Jos Brouwers
 MSc.-Eng. Przemek Spiesz
 Eindhoven University of Technology
 Faculty of the Built Environment
 P.O. Box 513
 5600 MB Eindhoven

Dr.Dipl.-Ing. Götz Hüsken
 BAM Federal Institute for Materials Research and Testing
 Division 7.1 Building Materials
 Unter den Eichen 87
 D-12200 Berlin